Journal of Applied Polymer Science

Structure-properties investigations in hydrophilic nanocomposites based on polyurethane/poly(2-hydroxyethyl methacrylate) semi-interpenetrating polymer networks and nanofiller densil for biomedical application

Panagiotis Klonos,[1] Vasileia Chatzidogiannaki,[1] Konstantinos Roumpos,[1] Ellas Spyratou,[1] Panayiotis Georgiopoulos,[2] Evagelia Kontou,[2] Polycarpos Pissis,[1] Yuriy Gomza,[3] Stanislav Nesin,[3] Oksana Bondaruk,[3] Lyudmyla Karabanova[3]

[1]Department of Physics, National Technical University of Athens, Zografou Campus, Athens 15780, Greece
[2]Mechanics Department, National Technical University of Athens, Zografou Campus, Athens 15780, Greece
[3]Institute of Macromolecular Chemistry, National Academy of Sciences of Ukraine, Kiev 02660, Ukraine
Correspondence to: L. Karabanova; (e-mail: lyudmyla_karaban@ukr.net)

ABSTRACT: Nanocomposites based on sequential semi–interpenetrating polymer networks (semi–IPNs) of crosslinked polyurethane and linear poly(2-hydroxyethyl methacrylate) filled with 1–15 wt % of nanofiller densil were prepared and investigated. Nanofiller densil used in an attempt to control the microphase separation of the polymer matrix by polymer–filler interactions. The morphology (SAXS, AFM), mechanical properties (stress–strain), thermal transitions (DSC) and polymer dynamics (DRS, TSDC) of the nanocomposites were investigated. Special attention has been paid to the raising of the hydration properties and the dynamics of water molecules in the nanocomposites in the perspective of biomedical applications. Nanoparticles were found to aggregate partially for higher than 3 and 5 wt % filler loading in semi–IPNs with 17 and 37 wt % PHEMA, respectively. The results show that the good hydration properties of the semi–IPN matrix are preserved in the nanocomposites, which in combination with results of thermal and dielectric techniques revealed also the existence of polymer–polymer and polymer–filler interactions. These interactions results also in the improvement of physical and mechanical properties of the nanocomposites in compare with the neat matrix. The improvement of mechanical properties in combination with hydrophilicity and biocompatibility of nanocomposites are promising for use these materials for biomedical application namely as surgical films for wound treatment and as material for producing the medical devises.

KEYWORDS: biomedical applications; dielectric properties; differential scanning calorimetry; hydrophilic polymers; polyurethanes

Received 10 June 2015; accepted 26 October 2015
DOI: 10.1002/app.43122

INTRODUCTION

Polymer nanocomposites have attracted significant attention for the last decades both from the academic and industrial point of view.[1–6] The main reason for that is the enhancement of mechanical, thermal and other properties of nanocomposites compared with those of their initial components[1,3,6] and those of conventional composites.[7] The use of nanoscale fillers (spherical nanoparticles,[8–11] CNTs,[5,6] nanosheets[9,12]) offers the great benefit that small amount of filler content is sufficient to induce tremendous improvements in desired properties, mainly due to the surface to volume ratio of the nanoparticles, which is very high in the nanocomposites, in comparison with conventional composites.[7] Thus, of great significance is the achievement of good/uniform dispersion of nanofillers. The dispersion of nanoparticles may be improved by additional functionalization of their surface to create covalent bonding with polymer matrix.[13,14]

Nanocomposites containing oxide nanoparticles, in particular silica, have been widely studied for the last years.[8,10,11] Such nanocomposites were prepared by sol–gel method,[15–20] the Stoeber method,[21] conventional mixing[12,22–24] and physical adsorption of the polymer onto the nanoparticles.[25–27] The interaction between filler and polymer occurs mainly via physical (mostly hydrogen) or/and chemical (covalent) bonding.[8,13,18]

Additional Supporting Information may be found in the online version of this article.

In our previous works,[23,28–34] morphology, dynamic–mechanical behavior, elastic and physico–mechanical properties, segmental mobility and hydration properties, have been studied in several polyurethane/poly(2-hydroxyethyl methacrylate) semi–interpenetrating polymer networks (PU–PHEMA semi–IPNs) over the temperature range from −140 to 180°C, by using combination of scanning electron microscopy (SEM), atomic force microscopy (AFM), dynamic mechanical analysis (DMA), laser–interferometric creep rate spectroscopy (CRS), differential scanning calorimetry (DSC), broadband dielectric relaxation spectroscopy (DRS, TSDC) and water sorption–desorption techniques (ESI, DSI). These systems have basically two–phase, nano–heterogeneous structure with incomplete phase separation, and pronounced dynamic heterogeneity within the extraordinarily broadened PHEMA and PU glass transitions. Such dynamic behavior and, additionally, improved biocompatibility of PU–PHEMA semi–IPNs, in combination with the chemically mild processing, good mechanical and thermochemical (non toxic) properties of silica,[8,10] are of interest for developing improved biomedical, damping or membrane materials.

In the present study we continue with the investigation of the nanocomposites based on PU–PHEMA semi–IPNs with various contents (1, 3, 5, 10, and 15 wt %) of modified fumed silica nanoparticles. The modification of silica has been obtained by the mechanochemical activation (MCA) of initial fumed oxides and resulted in surface's changes and significantly higher porosity of nanofiller.[35] The materials have been prepared and investigated having in mind biomedical applications, on the basis of biocompatibility of the PU and biocompatibility combined with strong hydrophilicity of PHEMA and silica.[34,36] To that aim we employ a combination of structure (Small Angle X–ray Scattering, SAXS), surface morfology (AFM), mechanical (stress–strain), calorimetric (DSC), and thermo–dielectric (broadband dielectric relaxation spectroscopy, DRS, and Thermally stimulated depolarization currents, TSDC) techniques. Especially in the perspective of biomedical applications significant effort has been paid to the hydration properties of the materials, that is, water uptake at different levels of water activity, diffusion of water and the effects of adsorbed water on the properties of the polymer matrix Thus, Equilibrium and Dynamic water Sorption/Desorption (ESI, DDI) techniques were also employed, whereas dielectric measurements were performed at varios levels of hydration.

EXPERIMENTAL

Materials and Preparation

Nanocomposite samples were prepared based on a multicomponent polymer matrix, namely semi–IPNs consisting of Polyurethane (PU) and Poly(2-hydroxyethyl methacrylate) (PHEMA). As nanofiller, densil was used. Densil is the product of nanosilica A–300 (~8 nm in diameter and ~50 g/dm^3 in density) modification by mechano–sorptive method.[14] The result of such modification is the changes in asperity of surface and porosity of nanofiller (densil, 325–330 g/dm^3 in density).[14]

Semi–IPNs, which were used as the matrix to create the nanocomposites, were obtained as follows. First, the polyurethane network was synthesized by a two–step method. The first step was the preparation of adduct of TMP and TDI. Adduct of TMP/TDI was synthesized by reaction of 1 g–eqiv of TMP with 1.5 g–eqiv TDI at 65°C. The reaction was carried out to achieve the theoretically calculated isocyanate group content, which was determined by titration method. The second step was the synthesis of three–dimensional polyurethane. The polyurethane network was obtained from a mixture of poly(oxypropylene glycol), POPG, of MM 2000 and adduct TMP/TDI (ratio 1:2 g–eqiv.) at 80°C in a nitrogen atmosphere.[23] The structure of PU network is presented in Scheme 1:

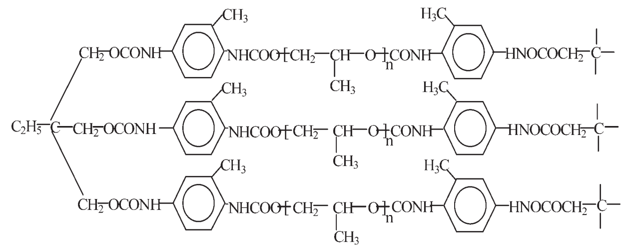

Scheme 1. The Structure of Polyurethane Network.

Semi–IPNs were obtained by a sequential method. Films of PU network were subjected to swelling in HEMA monomer containing photoinitiator. Swelling was carried out to equilibrium. Then the photopolymerization of monomer HEMA in the matrix of PU was carried out. The resulting second polymer, PHEMA, is presented in Scheme 2.

For creation of the nanocomposites the nanofiller densil was introduced into the polymer matrix during the stage of polyurethane synthesis at the amount of 1, 3, 5, 10, 15 wt %. Samples of nanocomposites were kept in vacuum (10^{-5} Pa) at 80°C for 36 h before reaching a constant weight. The composition of the polymer matrix used was fixed to 83 wt % PU – 17 wt % PHEMA, 63 wt % PU – 37 wt % PHEMA and throughout the text these matrices will be also named as semi–IPN17 and semi–IPN37, respectively.

Small Angle X–ray Scattering

The peculiarites of the microheterogeneous structure of the unfilled semi–IPNs and nanocomposites based on semi–IPNs have been investigated by small–angle X–ray scattering. Small angle X–ray scattering (SAXS) studies have been carried out with a vacuum Kratky camera. X–ray source was a CuK$_\alpha$ line monochromated with total internal reflection and nickel filters.[37] Data collection has been carried out in a regime of multiple step scanning of a scintillation detector in the range of scattering angles 0.03 to 4.0°, which corresponded to the values of wave vectors q of 0.022 to 2.86 nm^{-1} ($q=4\pi\cdot\sin\theta/\lambda$, where θ is a half of the diffraction angle 2θ, and λ is the wavelength of X–ray radiation emitted by the copper anode λ =0.154 nm). SAXS method is sensitive to local variations of the density due to presence of domains of higher than average density or voids with smaller than average density and distribution of such heterogeneity with characteristic dimensions (determined as $2\pi/q$) in the range of 2 to 280 nm. The initial treatment of the data has been performed with the FFSAXS program,[38] including the procedures of background noise subtraction, normalizing of the diffraction curves to the absolute values of scattering, and

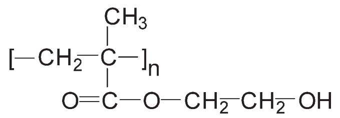

Scheme 2. The Structure of Poly(2-hydroxyethyl methacrylate).

application of collimation corrections. The treated diffraction curves were then used for calculations of the mean square fluctuations of the electron density and three dimensional correlation functions in accordance to the procedures described in Ref. 39.

Atomic Force Microscopy

Examination of the surface topography was performed by Atomic Force Microscopy (AFM)[40,41] for selected samples. AFM was performed using a Nanoscope diInnova (Veeco Metrology, Santa Barbara CA) with an Innova scanner possessing a maximum range of 100 × 100 × 7.6 μm. Phosphorus (n) doped silicon tips with a nominal constant range from 20 to 80 N/m were used. Measurements were performed in air by standard and intermittent (tapping) contact.

Mechanical Properties (Stress–Strain)

Tensile measurements were performed with an INSTRON 1121 tester at room temperature. The dumbbell type specimens were of a gauge length of 20 mm, and the applied crosshead speed was 0.5 mm/min. This value corresponds to an effective strain rate of 4.16×10^{-4} s^{-1}. The strain was being measured with a non–contact experimental procedure, employing a laser extensometer with very high accuracy.[42,43] Measurements were performed for samples based on semi-IPN with 17 wt % PHEMA. Three specimens of each of the five selected samples (totally 15 specimens) were tested, and average values are presented.

Differential Scanning Calorimetry

Differential scanning calorimetry (DSC) measurements were performed in nitrogen atmosphere in the temperature range from −120 to 230°C using a TA Q200 DSC instrument. Samples of about 8 mg in mass, cut from the produced films, were closed in standard Tzero aluminium pans. Cooling and heating rates were fixed at 10°C/min. During the first heating scan the samples were kept at 120°C for 2 min (isothermally) in order that water contained in the sample evaporates (scan 1). Then the samples were cooled down to −120°C and the second heating scan was recorded up to 230°C (scan 2). The DSC thermograms were evaluated in terms of the glass transition temperatures determined as the midpoint of the heat capacity step at glass transition and the corresponding heat capacity changes. The heat capacity change at glass transition, $\Delta C_{p,\mathrm{DSC}}$, was normalized to the respective polymer fraction (PU and PHEMA, X_{PU} and X_{PHEMA}, respectively, assuming complete microphase separation) depending on the process followed according to the following equation:

$$\Delta C_{p,\mathrm{norm}} = \frac{\Delta C_{p,\mathrm{DSC}}}{(1-X_{\mathrm{filler}})X_{\mathrm{PU/PHEMA}}}, \tag{1}$$

Dielectric Relaxation Spectroscopy

For dielectric relaxation spectroscopy (DRS) measurements[44,45] the samples (films of ~0.5 mm in thickness and 20 mm in diameter) were placed between the plates of a capacitor and an alternate voltage was applied in a Novocontrol sample cell. The complex dielectric permittivity, $\varepsilon^{*}=\varepsilon' - i\varepsilon''$, was recorded isothermally as a function of frequency in the range from 10^{-1} to 10^{6} Hz. The measurements were carried out in the temperature range from −150 to 120°C in steps of 5 and 10°C depending on the process followed. DRS measurements were carried out by means of a Novocontrol Alpha analyzer while temperature was controlled to better than 0.5°C by a Novocontrol Quatro cryosystem.

Equilibrium Water Sorption–Desorption Isotherms (ESI, EDI)

The isothermal sorption curves were determined at room temperature by exposing the samples to water vapor atmospheres in sealed jars.[46] The water activities *rh* were achieved with appropriate binary saturated aqueous solutions.[47] The samples were equilibrated for 6 days to water activities of 0.02 (phosphor pentoxide, P_2O_5), 0.19, 0.43, 0.64, 0.75, 0.85, and 0.95. The attainment of equilibrium was determined via recording of sample weight (m_{sample}). A Mettler Toledo balance with 10^{-5} g sensitivity was employed for these measurements. The weights of samples after equilibration over P_2O_5 were considered as weights in dry state ($m_{\mathrm{dry,sample}}$). Once the equilibrium was attained, the hydration ($h_{\mathrm{dry,basis}}$) was calculated on dry basis through the equation:

$$h_{\mathrm{dry,basis}} = \frac{m_{\mathrm{water}}}{m_{\mathrm{dry,sample}}} = \frac{m_{\mathrm{hydrated,sample}} - m_{\mathrm{dry,sample}}}{m_{\mathrm{dry,sample}}}, \tag{2}$$

Dynamic Water Desorption Isotherms

Dynamic water desorption isotherms (DDI) were also recorded while the samples, previously equilibrated at 0.95 *rh*, were allowed to equilibrate in the ambient humidity (about 0.4 *rh*). Measurements were performed using the high accuracy balance, as in ESI, and data (sample weight vs time) were collected with the use of a suitable computer software (Mettler Toledo). The diffusion coefficient of water, *D*, was calculated, employing the following equation[48]

$$\frac{(\Delta m)_t}{(\Delta m)_\infty} = \frac{4}{\sqrt{\pi}}\sqrt{\frac{tD}{l^2}}, \tag{3}$$

where $(\Delta m)_t$ is the change (increase or decrease) in the water mass on the sample after a time period t from the beginning of the measurement, $(\Delta m)_\infty$ is the respective value at equilibrium and l is the thickness of the sample. *D* was calculated by fitting the above equation to experimental data, assuming (a) Fickian behavior, (b) water diffusion in one direction through a certain surface of the sample (which is a thin film in the present study), and (c) unchanged thickness of the sample during the experiment.[19,34,48]

RESULTS AND DISCUSSION

Peculiarities of the Nanocomposites' Structure (SAXS)

In Figure 1(a) the small–angle scattering curves for the two semi–IPNs based on polyurethane and poly (2–hydroxyethyl methacrylate), containing 17 and 37 wt % of PHEMA, and for nanofiller densil are presented. The structure of semi–IPNs was investigated and described in detail in previous work.[49] It was shown that such materials are two–phase systems with

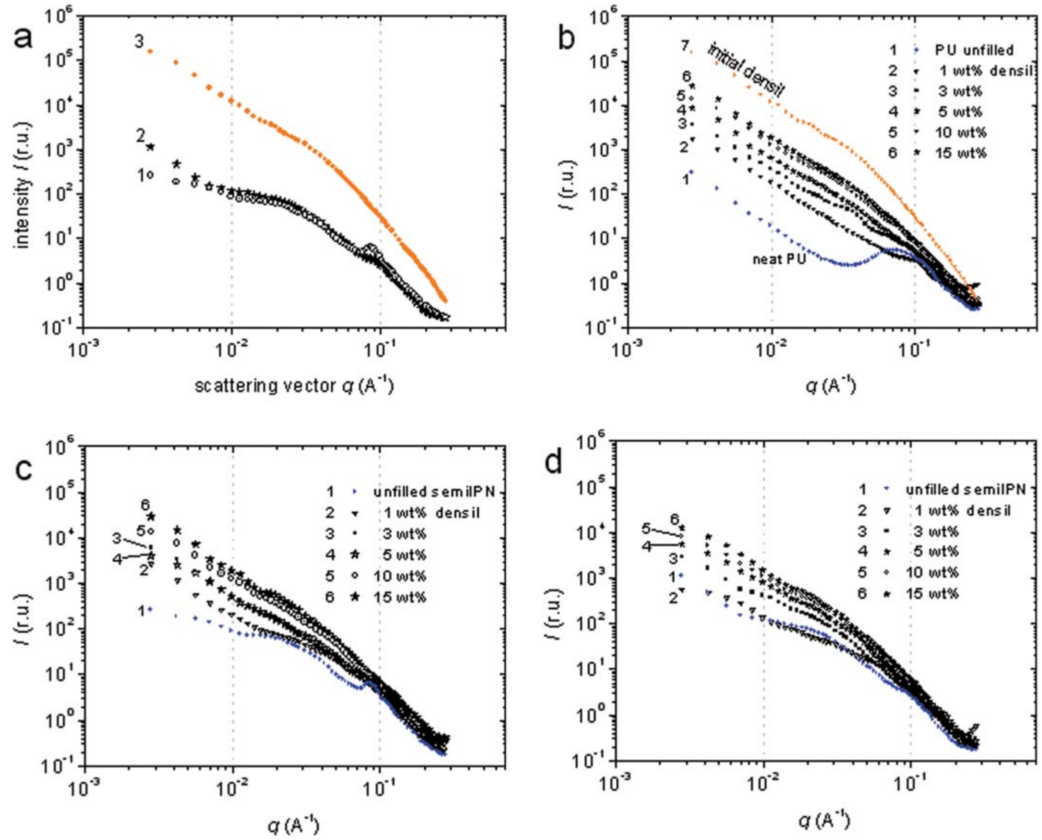

Figure 1. SAXS intensity $I(q)$ versus scattering vector q, for (a) semi–IPN with 17% PHEMA (1) semi–IPN with 37% PHEMA (2) and for nanofiller densil (3), and for the nanocomposites containing nanofiller densil based on PU (b) and semi–IPNs with (c) 17 wt % PHEMA and (d) 37 wt % PHEMA matrixes. The result for initial densil nanoparticles was added also in (b). [Color figure can be viewed in the online issue, which is available at wileyonlinelibrary.com.]

incomplete microphase separation and with the presence of two hierarchical levels of heterogeneity. The first level is the concentration fluctuations with sizes of 30–40 Å which are fixed in the early stage of spinodal decomposition, the second level of heterogeneity corresponds to later stages of microphase separation and it is characterized by the release of almost pure polyurethane microinclusions and PHEMA domains that include polyurethane chains.[49]

The main difference between the curves for the two semi–IPNs presented in Figure 1(a) is the different degree of expression of polyurethane diffraction peak, located at $q* = 0.8$. It is well defined for semi–IPN containing 17% PHEMA, and virtually traced for semi–IPN with a higher content of PHEMA.

Curve scattering by densil [Figure 1(a), curve 3] is characterized by two linear sections of intensity plot: the first one is in the range of q from 0.027 to 0.200 nm^{-1}, with a slope of -4.0, and the second one is in the range of q from 0.5 to 2.7 nm^{-1}, with a slope of -2.1. The value of the slope of the first section -4.0 reflects the presence of nearly smooth surface of nanofiller. The slope of the second section displays the mass–fractal nature of the aggregation of the primary particles of nanofiller.[50,51]

The plot kink between them (ranging q from 0.2 to 0.5 nm^{-1}) corresponds to the Guinier contribution, which allows to calculate the radius of gyration of the nanofiller's particle R_g assuming their spherical shape.[52] The calculations, carried out in accordance to the algorithm Guinier, gave values of $R_g = 5.0$ nm. For spherical particles this corresponds to a diameter $d_{sf} = R_g\ 2.58 = 12.9$ nm.

In Figure 1(b) the small–angle scattering curves for native polyurethane, for the nanofiller densil and for a series of nanocomposites containing densil from 1 to 15% by weight are presented. As could be seen from Figure 1(b), the curve for the native polyurethane is characterized by a diffraction peak with a maximum at wave vector value $q* = 0.8\ nm^{-1}$. This corresponds to a periodicity of $2\pi/q*$ equal to 7.9 nm, which corresponds to the spatial periodicity of microinclusions location enriched by rigid component.[37]

From Figure 1(b) it is evident that introduction of already a minimum amount of nanofiller densil into the polymer matrix, which is in this case the polyurethane, results in essential changes in small–angle scattering. The scattering intensity in the range of wave vector value $*q$ from 0.027 to 0.6 is substantially higher for the nanocomposite, as compared with the scattering intensity for the native polyurethane. Additionally, the polyurethane's dispersion maximum, observed on the curve of native polyurethane, almost completely disappears in the nanocomposite. With further increasing of the nanofiller content in the nanocomposites (3–15%) the systematic evolution of nanocomposite's curve dispersion to the curve characteristic for the nanofiller is observed.

That is, after introduction of nanofiller in quantities exceeding 3% we are able to detect on the scattering curves of the nanocomposites only this component, whereas the contribution of the polyurethane matrix becomes neglectly small. This reflects the fact that the level of scattering by the nanofiller is about three orders of magnitude higher than the scattering intensity by the polyurethane matrix.

For better understanding the nature of structural changes in the polyurethane matrix with the introduction of a minimum amount of nanofiller we should take into account the fact that the average size of nanofiller particles is approximately two times higher the value of spatial periodicity of the microregions location enriched by rigid component. It should also be noted that the introduction of the nanofiller occurs into the monomer mixture before polymer synthesis. This means that polyurethane formation occurs in the presence of nanofiller distributed in the reaction mass. The surface of nanofiller affects the formation of the polymer matrix. So, the fact of complete disappearance of polyurethane maximum on the curve of nanocomposite with 1% of nanofiller could be consider as indirect evidence of approximate uniform distribution of nanofiller in the bulk of the nanocomposite.

When the content of nanofiller in the polyurethane matrix increases from 3 to 15% the manifestations of polyurethane diffraction peak on the corresponding scattering curves disappear completely. The scattering curves of nanocomposites, like the original scattering curve of nanofiller densil [Figure 1(a), curve 3], are characterized by the presence of two linear sections. Table I shows the values of slopes of the linear sections.

As could be seen from Figure 1(b) and Table I, the value of slope S_2 is -1.8 for the nanocomposite with filler content 1% and comes close to -2.1, which is the value for native densil, by increasing the nanofiller content from 3 to 15%. At the same time there is a gradual transition of the scattering curves of the nanocomposites in Figure 1(b) to the curve characteristic of pure nanofiller. This fact can be interpreted in favour of the assumption of a process of loosening of nanofiller's aggregates at 1% filler content, and the almost complete preservation of the character of its aggregation at concentrations of nanofiller ranging from 3 to 15% in the nanocomposites.

From the above presented analysis we could suggest homogeneous distribution of nanofiller in the nanocomposite at its minimum content (1%) and its aggregation with content of nanofiller exceeding this value (3–15%) in the nanocomposites.

Let us discuss now the structural features of the nanocomposites based on the multicomponent polymer matrix, which is a semi–IPN consisting of the polyurethane network and linear PHEMA. In Figure 1(c) the scattering curves for semi–IPN with 17% PHEMA (semi–IPN17) and for the nanocomposites based on this semi–IPN containing from 1 to 15% of densil are presented. As could be seen from Figure 1(c), the introduction of the minimum amount of nanofiller fundamentally changes the nature of the scattering intensity curve of the nanocomposite

Table I. Values of the Slopes of the Linear Sections of Small–Angle X–ray Scattering (SAXS) Curves

Samples	Filler content (wt %)	S_1 (slope)	S_2 (slope)
Densil	100	−4.0	−2.1
PU neat	0	−2.7	−1.8
PU + 3% densil	3	−3.0	−2.1
PU + 5% densil	5	−3.5	−2.1
PU + 10% densil	10	−3.3	−2.0
PU + 15% densil	15	−3.3	−2.1
semi–IPN17 neat	0	−3.3	−1.8
semi–IPN17 + 3% densil	3	−3.5	−1.9
semi–IPN17 + 5% densil	5	−3.6	−2.0
semi–IPN17 + 10% densil	10	−3.7	−2.0
semi–IPN17 + 15% densil	15	−3.7	−2.1
semi–IPN37 neat	0	−3.0	−1.3
semi–IPN37 + 3% densil	3	−3.0	−1.5
semi–IPN37 + 5% densil	5	−3.5	−1.7
semi–IPN37 + 10% densil	10	−3.7	−1.7
semi–IPN37 + 15% densil	15	−3.7	−1.8

compared with the scattering intensity curve of the native polymer matrix, similar to the case of pure polyurethane matrix [Figure 1(b)]. The diffraction maximum of polyurethane disappears almost completely in the nanocomposites, the level of scattering in the initial region of the curve significantly increases (in the range from minimum to 0.07 nm^{-1}), and also the maximum of semi–IPN located at $*q = 0.25\ nm^{-1}$ reduces. Further increasing of nanofiller content in the semi–IPNs, as in the case of polyurethane matrix, leads to the kind of dispersion curve, which is close to the native nanofiller.

Table I shows the values of the slopes of the two linear sections of the scattering curves observed in Figure 1(c). Comparison with the corresponding values of the slopes for the nanocomposites based on the polyurethane matrix, leads to the conclusion about the expansion of the limit of homogeneous nanofiller distribution from 1% (in the case of polyurethane matrix) to 3% (in the case of semi–IPN17 as a matrix).

The results for the nanocomposites based on the semi–IPN containing 37% of linear PHEMA as matrix are presented in Figure 1(d). As could be seen, for the native polymer matrix, unlike the previous matrices, only traces of the polyurethane diffraction peak (in the range of wave vector value about 1.0 nm^{-1}), so that it makes no sense to attribute them to any spatial periodicity. At the introduction of 1% of nanofiller into this polymer matrix, the traces of polyurethane diffraction peak disappear completely, similar to the case of the semi–IPN17 matrix. The main difference in the results of the investigation of this system and the nanocomposite based on the semi–IPN17 is the following. For the nanocomposite based on semi–IPN17 containing 1% of nanofiller a significant excess of scattering was observed, as compared with the unfilled system [Figure 1(c)]. For the nanocomposite based on semi–IPN37, on the contrary, changes are hardly observed: the scattering curve for the nanocomposite containing 1% nanofiller is very close to the scattering curve for the native polymer matrix [Figure 1(d)].

This result could be the indirect evidence that in the matrix of semi–IPN37 the nanofiller is distributed not only in the flexible part of the polyurethane component (as in the case of nanocomposites based on polyurethane matrix), but also in the domains containing linear PHEMA. Analysis of the changes of the slope of the second linear section of the scattering curves with concentration (Table I) is in favor of the assumption of further homogenization of nanofiller distribution in the nanocomposites based on semi–IPN37 in the region up to 5% nanofiller content. The values of the mass–fractal dimension of nanofiller aggregates are much lower for the nanocomposites based on semi–IPN37 than those observed for semi–IPN17.

Thus, the investigation of the structural features of the binary nanocomposites polyurethane–densil allows the following conclusions about the behavior of nanofiller particles in the system. Nanofiller at minimum content (1%) is almost uniformly distributed in the polyurethane matrix, while by increasing its content in the matrix, aggregation occurs in the form of mass–fractal structures, typical for native nanofiller. When we use the multicomponent polymer matrix (semi–IPN) the second polymer component in the matrix promotes the homogenization of nanofiller distribution in case of PHEMA 17 from 1 to 3%, and in the case of PHEMA 37 – from 1 to 5%. Raising the threshold of homogenization of nanofiller distribution is the result of reorganization of filled polyurethane during the process of formation of nanocomposites based on the multicomponent polymer matrix. When the swelling of filled polyurethane with the monomer HEMA occurs during the formation of nanocomposites, destruction of loose aggregates of nanofiller and improvement of its uniform distribution could take place. The uniform distribution is further supported by photopolymerization of the monomer HEMA. On the basis of these results, we could assume optimum physical and mechanical properties of the systems where the concentration of nanofiller is near its respective threshold for aggregation (i.e., 1% for the nanocomposites with polyurethane matrix, 3% for those with semi-IPN 17 matrix, and 5% for those with semi-IPN 37 matrix).

Surface Topology (AFM)

By employing AFM of intermittent contact (tapping) mode[40,41] for unfilled PU–PHEMA semi–IPN with 17 and 37 wt %) of PHEMA (not shown), well defined structures (2–6 μm in size) were recorded along the surfaces and the inner volume.

Employing the ability of AFM under tapping mode to sense qualitative changes on surface micro–hardness[53–56] and comparing the AFM response of semi–IPNs with initial PU and initial PHEMA, we suggest that the 2–6 μm structures correspond to micro-separated Polyurethane phase, while the material in the area between these structures consists of mixed PU and PHEMA.

Comparing now the semiIPNs of different compositions, in the case of semi–IPN37 the surface of the samples is smoother and the concentration and size of Polyurethane structures is lower (2–4 μm in size), as compared to semi–IPN17 (rather diffused surfaces, 4–6 μm Polyurethane structures). This result is in agreement with SAXS data,[49] because with decreasing amount of PU in the semi-IPNs, the ordering part of this polymer also decreases in the structure of semi-IPNs.

Differences in the hardness of the mixed PU–PHEMA phases between 17 and 37 wt % PHEMA and initial PU could not be further evaluated. The above observations suggest that PU–PHEMA mixing is possibly higher for semi–IPN37, or, in other words, PHEMA–PU microphase separation is higher in semi–IPN17, taking into account the existing of ordering part of PU in the structure of semi-IPNs. Figure 2 shows AFM under contact mode images for selected semi–IPN nanocomposites. It can be easily observed that filler is well distributed in the structure of semi–IPN17 filled with 1 wt % densil, while for 5 wt % and higher of filler content densil is highly aggregated in structures up to 500 nm in size.

Results for such filler distribution are similar for semi–IPN37 (not shown) and are in agreement with the observations of filler aggregation obtained by SAXS investigations of these nanocomposites. Coming now to the highest filler content, that is, 15 wt % densil, we see in Figure 2(c) that in semi–IPN17 the aggregates of densil are almost connected in a branched network in the structure of the sample. The result is not similar in the case of semi–IPN37 filled with 15 wt % densil, for which large separately distributed densil aggregates are observed in Figure 2(d). Such distribution of densil in semi-IPN37 could be explained by peculiarities of nanocomposites preparation. During process of filled polyurethane swelling the monomer HEMA mainly concentrated in the parts of polyurethane free of densil aggregates and, after photopolymerization of monomer HEMA in the matrix of filled PU, we could observe destroyed branched network of nanofiller. Instead of branched network of nanofiller the large separately distributed densil aggregates are observed in the structure of semi–IPN37 filled with 15 wt % densil, which is characterized by more smooth areas enriched by PHEMA.

In previous studies of poly(2-hydroxyethyl acrylate)/poly(ethyl acrylate) copolymers[14,46,57] and polydimethylsiloxane[18] both filled with silica nanoparticles *in situ* generated via sol–gel technique, silica was also found to form a network for contents above about 10 wt %. The presence of this network affected significantly the mechanical and swelling properties of the polymer (in water and, in general, polymer solvents).

Physico–Mechanical Properties of the Nanocomposites

Results of stress–strain testing for samples based on semi–IPN17 are presented in Figure 3. It can be seen that the introduction of densil into the polymer matrix leads to significant increase of physical and mechanical parameters of the nanocomposites in comparison with the neat matrix. However, the enhancement of physical and mechanical properties is non monotonous with the increase of the amount of nanofiller.

For 3% densil in the polymer matrix (Figure 3, curve 2) the increase of stress at break and elongation at break of the

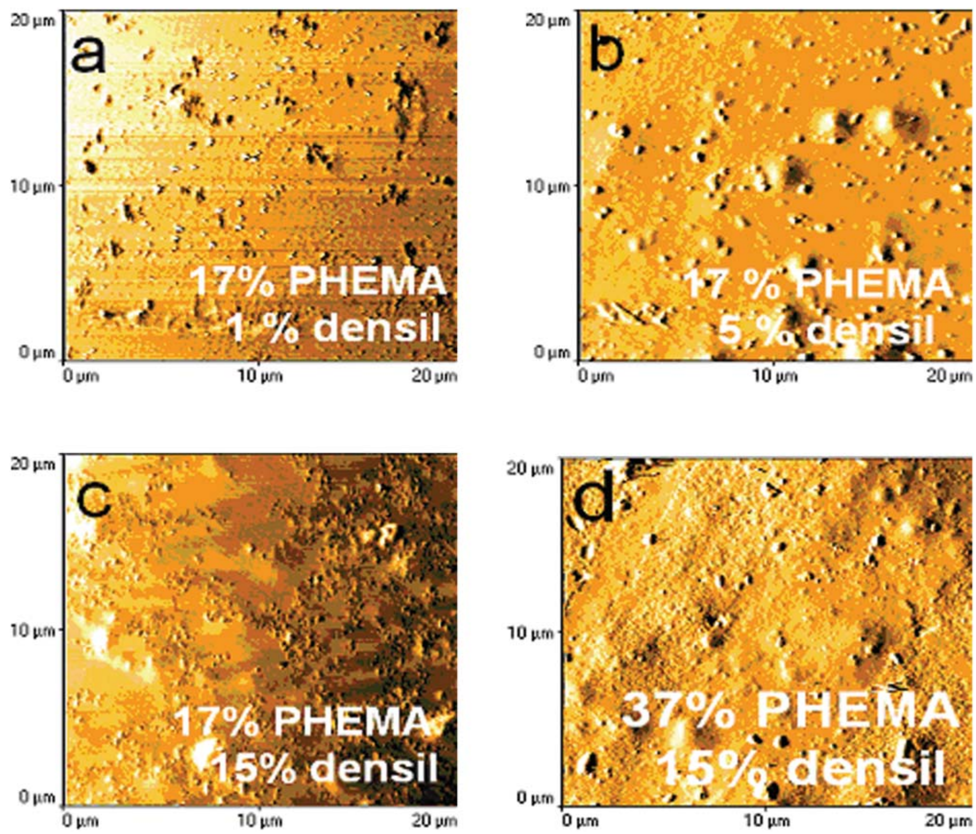

Figure 2. AFM images by standard contact mode for semi–IPNs with 17 wt % PHEMA filled with (a) 1 wt % densil, (b) 5 wt % densil and (c) 15 wt % densil, in the range of 20 × 20 μm^2. (d) Shows the AFM image for semi–IPN with 37 wt % PHEMA filled with 15 wt % densil. [Color figure can be viewed in the online issue, which is available at wileyonlinelibrary.com.]

nanocomposite compared with the matrix (Figure 3, curve 1) is observed. With increase of the filler content up to 5% (Figure 3, curve 3) the nanocomposite shows a sharp increase in stress at break, but the elongation at break is reduced relative to the matrix. This sample shows the maximum value of Young's modulus. The latter could indicate a uniform distribution of nanofiller particles densil in the nanocomposites containing 3–5%. With increase of filler content up to 10% (Figure 3, curve 4) reduction of stress at break and elongation at break of the nanocomposite is observed, both possibly arrising from increased filler aggregation. For 15% filler (Figure 3, curve 5), although elongation at break increases not significantly, the respective stress at break is increased by almost 30%. This could be explained in terms of the growth of a continuous densil structure (network) across the volume of this sample, in agreement with AFM result [Figure 2(c)].

In general, improvement of physical and mechanical properties of the nanocomposites in comparison with the neat matrix was observed: Stress at break increased by 30–135% and Young's modulus increased by 85–390% with nanofiller amount. The improvement confirms that nanofiller densil could be used as reinforsing nanofiller for the investigated and other systems.

Glass Transition (DSC)

Aiming at the investigation of polymer composition and filler content effects on the glass transition, without the interference of water, we used DSC results of the second heating scan from −110 to 220°C. Figure 4 shows DSC results for neat polymers and neat semi-IPNs along with the results for selected nanocomposites, that is, for 15 wt % densil. All the measured and

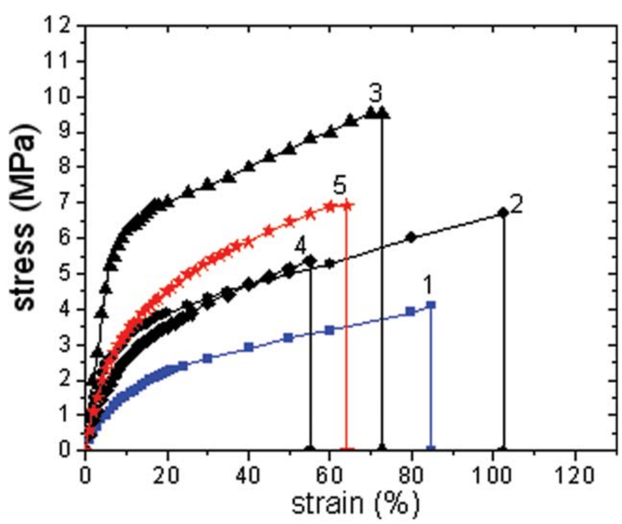

Figure 3. Stress–Strain curves for semi–IPN with 17 wt % PHEMA (1) and its nanocomposites filled with 3 wt % (2), 5 wt % (3), 10 wt % (4) and 15 wt % (5) of densil. [Color figure can be viewed in the online issue, which is available at wileyonlinelibrary.com.]

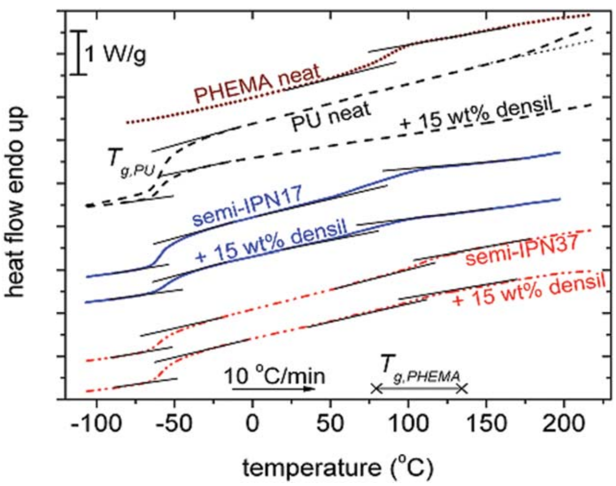

Figure 4. Comparative DSC thermograms of dried (dashed) PU and PU/15%densil, (solid lines) semi–IPN17 and semi–IPN17/15%densil and (dash-dotted lines) semi–IPN37 and semi–IPN37/15%densil, during heating. Included is the result for neat PHEMA (dotted line). The added lines represent the baselines of the thermograms before and after glass transition(s). [Color figure can be viewed in the online issue, which is available at wileyonlinelibrary.com.]

calculated parameters for the semi-IPNs and for the nanocomposites are shown in Table II. For both the unfilled matrices and for the nanocompo-sites two well separated endothermic steps at around −58 and 100°C were recorded (Figure 4), representing the glass transition of PU and PHEMA,[34,58,59] respectively.

Comparing with neat PU and PHEMA the respective T_g values of these components were found in semi–IPNs rather similar for PU and higher for PHEMA, especially for semi–IPN37 (Table II). The existence of two separate glass transitions of polymers in the mixture is a general indication of low degree of mixing between these polymer components. Exceptional is the behavior for semi-IPN17 filled with 15 wt % densil for which $T_{g,\mathrm{PHEMA}}$ is the lowest among all the compositions. Focusing now on changes in the heat capacity during glass transition, $\Delta C_{p,\mathrm{norm}}$ [eq. (1)], for semi–IPN17, $\Delta C_{p,\mathrm{norm,PU}}$ is similar with that of neat PU, but $\Delta C_{p,\mathrm{norm,PHEMA}}$ is by a factor of about 4 lower than in neat PHEMA (Table II). On the other hand for semi–IPN37, $\Delta C_{p,\mathrm{norm,PU}}$ is slightly higher that of neat PU, while $\Delta C_{p,\mathrm{norm,PHEMA}}$ is lower than in neat PHEMA. This could sugest that the mobility of PHEMA chains in the semi-IPNs is partly suppressed.

As could be seen from Table II the glass transition temperature of neat PU and of PU in the nanocomposites is about the same. This could suggest that nanofiller densil concentrated mainly around hard segments of PU forming hydrogen bonding between isocyanate groups of PU and silanol groups of densil. As a result, the soft segment of PU is not influenced by nanofiller and segmental motion in neat PU and in the filled PU remains unaffected. We could observe also that the glass transition temperature of PU in the semi-IPN17 and in the semi-IPN37 is the same with that in neat PU.

Introduction of nanofiller densil into the semi-IPN17 leads to inceasing T_g of PU from −58 to–52°C with the amount of nanofiller. This means that the soft segment of PU became

Table II. Glass Transition Temperatures, T_g, Normalized Heat Capacity Step at Glass Transition, $\Delta C_{p,\mathrm{norm}}$, of PU and PHEMA in the Neat Matrixes and in the Nanocomposites

Sample	$T_{g,PU}$ (°C)	$\Delta C_{p,norm,PU}$ (J/g°C)	$T_{g,PHEMA}$ (°C)	$\Delta C_{p,norm,PHEMA}$ (J/g°C)
PHEMA neat	–	–	88	0.19
PU neat	−58	0.47	-	-
PU + 3% densil	−58	0.46	-	-
PU + 5% densil	−58	0.43	-	-
PU + 10% densil	−59	0.44	-	-
PU + 15% densil	−58	0.45	-	-
semi-IPN17 neat	−58	0.47	89	0.05
semi-IPN17 + 3% densil	−57	0.45	90	0.03
semi-IPN17 + 5% densil	−56	0.44	94	0.02
semi-IPN17 + 10% densil	−54	0.44	94	0.01
semi-IPN17 + 15% densil	−52	0.43	79	0.04
semi-IPN37 neat	−58	0.56	102	0.13
semi-IPN37 + 3% densil	−57	0.57	114	0.20
semi-IPN37 + 5% densil	−59	0.53	106	0.14
semi-IPN37 + 10% densil	−57	0.58	110	0.17
semi-IPN37 + 15% densil	−58	0.49	110	0.20

$T_{g,PU}$ measured with accuracy 1°C.
** $\Delta C_{p,norm,PU}$ calculated with accuracy 0.02 J/g°C.
*** $T_{g,PHEMA}$ measured with accuracy 2°C.
**** $\Delta C_{p,norm,PHEMA}$ calculated with accuracy 0.02 J/g°C.

more "rigid" due to the presence of nanofiller. As shown by SAXS investigation, the nanofiller at concentrations above 5% creates aggregates with size larger than the size of hard segment of PU. As a result, these aggregates disturb also part of the soft segments which are close to netwok junctions. The "unfreezing" of segmental motion of segments close to aggregates of nanofiller occurs at higher temperatures in comparison with free soft segments and we observe shift of T_g of PU in these nanocomposites to higher temperatures.[60]

Concerning the nanocomposites based on semi-IPN37, T_g of PU in these nanocomposites is similar to neat PU and to nanocomposites based on PU matrix. According to SAXS data the size of aggregates of nanoparticles in these nanocomposites is smaller in comparison with nanocomposites based on semi-IPN17. So, the soft segments of PU in the nanocomposites based on semi-IPN37 are not disturbed by the aggregates of nanoparticles and T_g of PU is about the same with that in neat PU.

As could be seen from Table II, the glass transition of neat PHEMA is 88°C. It is approximately the same in the semi-IPN17, and essentially higher (102°C) in semi-IPN37. As was shown by our previous investigations,[29,60] during the process of network formation the monomer HEMA could create covalent bonding between its hydroxyls and residual isocyanate groups of PU resulting in grafting of HEMA on polyurethane network. As segmental motion is a cooperative process, PHEMA chains with constrained dynamics contribute to glass transition resulting in increasing of T_g in semi-IPN37. For small amount of PHEMA in semi-IPN17 such effect of constrained dynamics is negligibly small.

Introduction of nanofiller densil into the semi-IPNs leads to increasing of PHEMA T_g in both cases of semi-IPN17 and semi-IPN37 (Table II). This could suggest that during the processes of filled polyurethane swelling with monomer HEMA and the subsequent photopolymerization, HEMA could create layers on the surfase of nanofiller particles with high density and hydrogen bonding with this surface. This would imply additional constraints to segmental motion of PHEMA in the nanocomposites, resulting in the increasing of PHEMA's T_g with the amount of nanofiller.

As could be seen from Table II, the addition of densil into the semi-IPN17 up to 10 wt % results in increased $T_{g,\mathrm{PHEMA}}$ values and, at the same time, in systematically decreased $\Delta C_{p,\mathrm{norm,PHEMA}}$. This is additional indication of the densil–PHEMA interaction in the nanocomposites leading to suppression of mobility of PHEMA chains which create hydrogen bonding with the surface of nanofiller.

An interesting point for discussion is the response of semi–IPN17 filled with 15 wt % densil. $T_{g,\mathrm{PHEMA}}$ for this sample is the lowest and $\Delta C_{p,\mathrm{norm,PHEMA}}$ is the highest (Table II) among the nanocomposites under investigation. Taking into account the increase of PU's T_g in this nanocomposite, we would suggest the highest degree of PU-PHEMA mixing in this sample and, as a result, mutual influence on T_g's of the two components.

This result indicates also the low degree of PHEMA–densil interaction in this nanocomposite. Investigations by SAXS, AFM and stress–strain results confirm the formation of a silica network at 15 wt % densil content. Such network could offer minimum of silica free surface for interaction with PHEMA in comparison with other nanocomposites.

Finally, in a previous study of ours on same PU–PHEMA matrix filled with different nanosilicas (initial and surface modified A–300)[34] the existence of both polymer–filler and polymer–polymer interactions were also manifested in water immersion experiments. After long stay (6–130 days) of the samples in distilled water it was found that neat PU network was decomposed (hydrolyzed) by ~50–90%. PU decomposition was strongly suppressed, initially, with the addition of PHEMA and, further, at the presence of nanosilica (initial A–300 and surface modified A–300).

Local and Segmental Dynamics of the Polymers

Dielectric Relaxation Spectroscopy. Dielectric relaxation spectroscopy (DRS) results were recorded in the form of frequency dependence of the imaginary part of dielectric permittivity (related to dielectric losses), ε'' for selected temperatures (raw data are in Supporting Information S3). Data have been further analyzed by fitting model functions to the data (i.e., the Havriliak–Negami and Cole-Cole equations)[45,61–63] and will be presented and discussed here in terms of time scale (temperature dependence of frequency maxima) comparatively in Figure 5 (Arrhenius Plot).

DSC and TSDC data are also included in the Arrhenius plot at the equivalent frequencies of 1.6×10^{-3} Hz and 10^{-2} Hz, respectively.[20] TSDC is a special dielectric technique in the temperature domain, characterized by high sensitivity and high resolving power, the latter arising from its low equivalent frequency ($10^{4}-10^{2}$ Hz).[44] Raw TSDC data are shown in Supporting Information (Figures S1 and S2). We have chosen not to describe in detail the procedure of analysis and to discuss basic results on time-scale and dielectric strength of the relaxations.

Local Dynamics. In Figure 5, γ_{PHEMA} relaxation is assigned to rotation of hydroxyethyl groups in the side chain of PHEMA.[34] $\beta_{\mathrm{sw,PHEMA}}$ is a local secondary relaxation assigned to crankshaft motion of the PHEMA side groups with attached water molecules.[33,34,36] These relaxations along with their dependence on water content[19,36,46] were followed in detail here also by TSDC (Supporting Information Figure S1). In addition to these processes, we were able to follow by DRS γ_{PU} process, which is assigned to the crankshaft motion of the methylene sequences in the PU structure, and β_{PU} process, which is assigned to rotation of the polar carbonyl groups in the chemical structure of PU with attached water molecules.[58,61] Both γ_{PU} and β_{PU} dominate the response for PU and PU/densil samples (Supporting Information Figure S3), with no significant effects of filler loading. On the other hand, the response of both semi–IPNs is dominated by γ_{PHEMA} and $\beta_{\mathrm{sw,PHEMA}}$ relaxations, which are much stronger than γ_{PU} and β_{PU}. The analysis of the results showed also that the DRS spectra for semi–IPNs (Supporting Information Figure S3) are superpositions of both PU and PHEMA secondary relaxations (i.e., in total four processes).

Exploiting the power of analysis of isothermal results, it was revealed that the γ_{PHEMA} relaxation immigrates toward lower

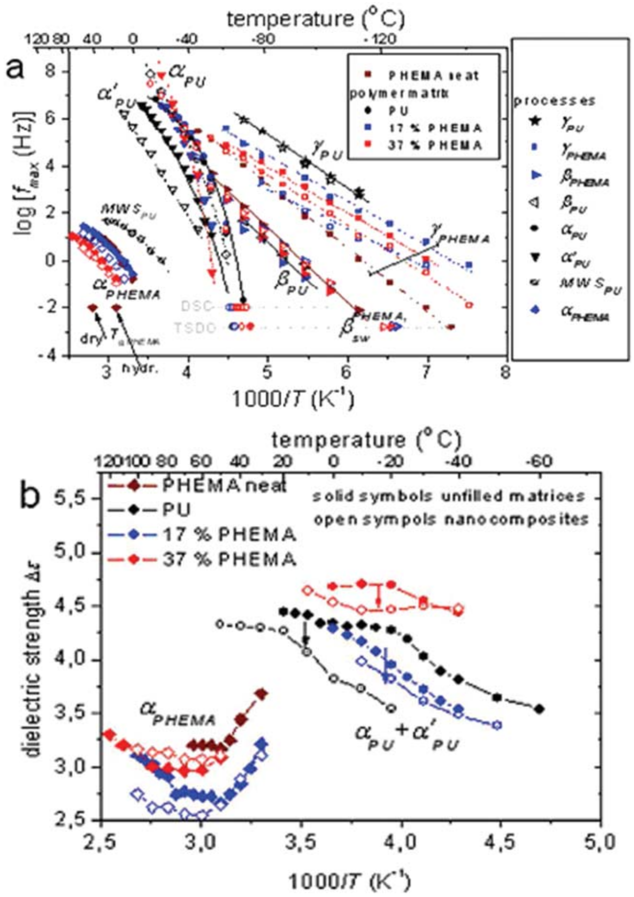

Figure 5. (a) Arrhenius plot of the segmental and local molecular dynamics and (b) dielectric strength for segmental relaxations of PU ($\alpha_{PU} + \alpha'_{PU}$) and PHEMA ($\alpha_{PHEMA}$), for neat PHEMA, neat PU, unfilled semi–IPNs and nanocomposites with 10 wt % densil. Solid and open symbols are used for unfilled polymers and nanocomposites, respectively. Each color is used for the samples based on the same polymer matrix, while each process (relaxation) is represented by specific type of symbol (star, square, triangle, cycle etc.) TSDC and DSC data are also included in the plot at the respective equivalent frequencies (details in text). The lines in (a) are fittings of the Arrhenius and the VTFH equations to the data, whereas in b they simply connect the data. [Color figure can be viewed in the online issue, which is available at wileyonlinelibrary.com.]

frequencies [becomes slower, Figure 5(a)] and simultaneously its dielectric strength decreases (becomes weaker, not shown) with densil loading (which can be explained in terms of the assignment of the secondary relaxation of PHEMA and the increased water content in the nanocomposites), whereas the respective effects on the β_{PU}, γ_{PU}, and γ_{PHEMA} relaxations are negligible.

Data for the time scale of relaxations are typically fitted in the literature by the Arrhenius equation (linear behavior in Arrhenius plot) in the case of secondary relaxations and by the Vogel–Tammann–Fulcher–Hesse equation (nonlinear behavior) in the case of primary relaxations,[34] reflecting the cooperative character of the latter against the non–cooperative one of the former.[64] In consistency with that, the data for the secondary relaxations could be well fitted by the Arrhenius equation, characteristic for local processes activated over a potential barrier.[64]

Segmental Dynamics of PU (a_{PU} Relaxation). We will now draw our attention on segmental dynamics, associated with the glass transition (dynamic glass transition). In agreement with DSC and TSDC results, the time scale of the α_{PU} and α'_{PU} relaxations [Figure 5(a)] was found to be practically independent of composition (presence of PHEMA and silica nanoparticles), as well as of water content, again with the exception of unfilled semi–IPN37 [see Figure 5(a)]. The mean values of dielectric strength, $\Delta\varepsilon$, of PU segmental relaxations for unfilled polymers do not change systematically with PU content [Figure 5(b)], although a slight suppression with filler addition is observed (in contradiction to TSDC). It is interesting to discuss the increase of $\Delta\varepsilon$ with temperature (in contradiction to what is observed in a glass forming liquid) which suggests the gradual loosening of constraints imposed to PU chain mobility by hard PU domains and PHEMA (glassy at these temperatures).[65]

Segmental Dynamics of PHEMA (a_{PHEMA} Relaxation). Finally, after careful analysis of DRS isotherms at higher temperatures (above 40°C), a region dominated by strong conductivity related phenomena (also for TSDC in Supporting Information Figure S1), we were able to record and demonstrate the time scale of the dynamic glass transition of PHEMA [i.e., α_{PHEMA} relaxation, Figure 5(a)] for all samples. As could be seen α_{PHEMA} is faster [Figure 5(a)] and stronger [Figure 5(b)] for neat PHEMA as compared to other compositions suggesting the possible suppression of its dynamics and strength, due to interactions with PU and densil (Table II). The effect on time scale is stronger for semi–IPN37 and the respective nanocomposites [Figure 5(a)].

These qualitative changes are in very close agreement to changes observed before from DSC (Table II), but we should note that the experimental DRS points in Figure 5(a) are at significantly lower temperatures (high frequencies) than those obtained with DSC. Finally, we should also report that additional conductivity effects imposed by densil arise further the uncertainity of recording and safe analysis of dielectric strength of α_{PHEMA} for the nanocomposites.

Hydration Properties and Water Diffusion in the Nanocomposites

Equilibrium Water Sorption Isotherms (ESI). Figure 6(a) presents the results of ESI measurements comparatively for neat nanooxides of densil and unmodified silica A–300.[34] Hydration, $h_{dry,basis}$ [eq. (2)], of initial filler is typical for fumed silicas[34] being of class III in the Brunauer classification,[19] which describes adsorption onto adsorbents with weak adsorbate–adsorbent interactions. $h_{dry,basis}$ is remarkably higher and of different pattern as compared to silica prepared by Sol–Gel technique [Figure 6(a), class I in the Brunauer classification].[19] Hydrophilicity of densil is slightly increased in the overall range of *rh*, as compared to unmodified A–300. This result suggests that the mechanochemical activation (MCA) of silica has increased the concentration of potential contact points of silica with water molecules (primary hydration sites, that is, silanol groups, Si–OH).[28,59] The similar for densil and silica A–300 increase of $h_{dry,basis}$ at high values of *rh*, that is, where formation

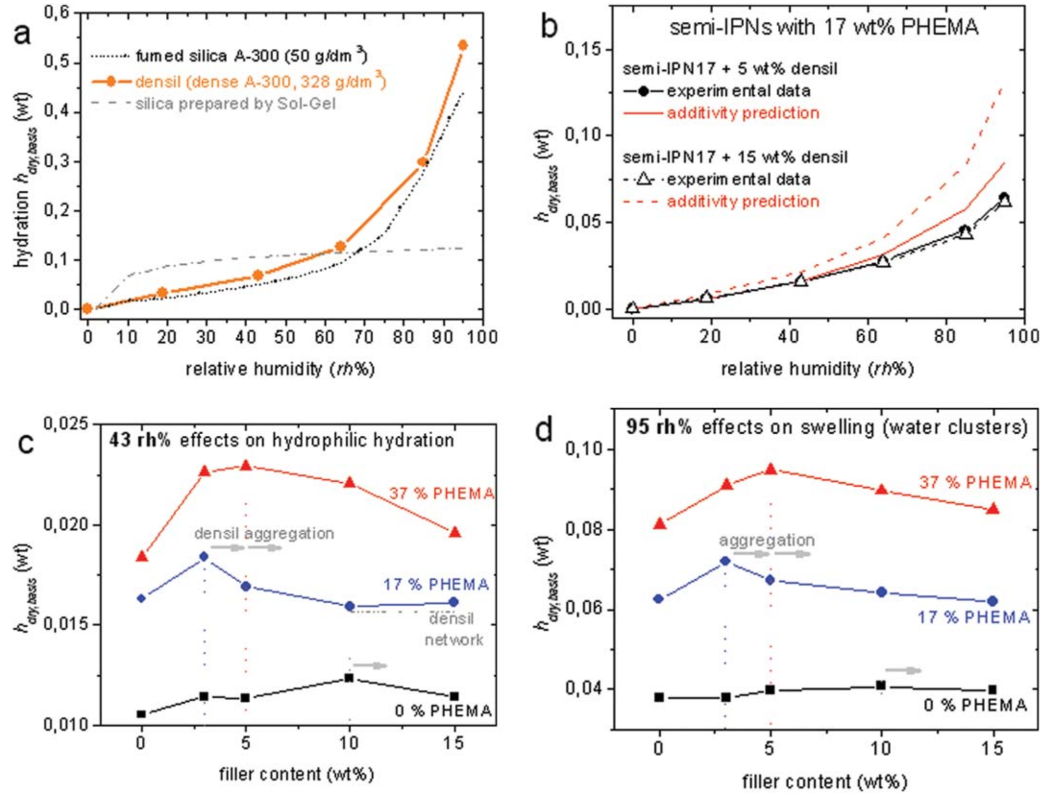

Figure 6. (a) Comparative ESI measurements of initial nanooxides: densil (solid cycles), fumed silica A–300 (dotted lines)[34] and silica nanoparticles prepared by Sol–Gel (dashed-dotted lines).[19] (b) shows comparative curves of experimental and calculated (additivity) ESI results between nanocomposites with 5 and 15 wt % densil based on semi–IPN17 matrix. (c,d) show hydration against filler content for densil nanocomposites based on PU (squares), semi–IPN17 (cycles) and semi–IPN37 (triangles) matrices; comparison between (c) intermediate (∼43 *rh*%) and (d) high (95 *rh*%) hydration contents. The lines simply connect the experimental points. The arrows mark the densil contents above which significant changes on hydration trends start. [Color figure can be viewed in the online issue, which is available at wileyonlinelibrary.com.]

of water clusters is expected,[36,46] suggests that the contribution of possible changes in porosity of silica (textural or intra–particle) on hydration[35] is possibly of lower significance.

Results of ESI measurements for all the samples studied in this work are shown in supplementary material (Supporting Information Figure S4), that is, neat PU and PHEMA, unfilled semi–IPNs and four nanocomposites based on the PU, semi–IPN17 and semi–IPN37 filled with densil (at the amounts of 3, 5, 10, and 15 wt %). The filler used in this work seems to be the most hydrophilic component among all the other components in the present systems (as shown in Supporting Information Figure S4). In Figure 6(b) experimental data of ESI measurement for two nanocomposites based on semi-IPN17 matrix are presented. The water sorption isotherms of neat semi-IPNS and their respective nanocomposites are also of class III in the Brunauer classification.[19] For the samples based on semi-IPN matrix, a steep increase of water content is observed at *rh* values above ∼0.6, reflecting the completion of the first hydration layer (bound water) and the formation of clusters around the primary hydration sites (semi–bound and free water).[34]

The unfilled semi-IPNs and all nanocomposites adsorb larger amounts of water as compared to neat PU and significantly lower as compared to neat PHEMA (Supporting Information Figure S4). We should keep in mind that sorption of PHEMA depends on density of crosslinks. According to DSC PHEMA in the semi–IPNs was found to be grafted with PU.[29]

ESI results are settled in three groups, promoting directly the effect of PHEMA content on hydration. Hydration levels of the unfilled semi–IPNs are similar to predicted values by additivity for sorption at low *rh* [Figure 6(b)], although being slightly lower for semi–IPN37 (not shown).

Bearing in mind that by calculating additive values we assume complete microphase separation and that we used for the PHEMA phase experimental data for crosslinked PHEMA, these results can be rationalized on the basis of higher hydrophilicity of the linear PHEMA used in this work, as compared to crosslinked PHEMA.

Coming now to the effects of filler, the striking result is that for both semi–IPN matrices at high levels of *rh* the experimental hydration levels deviate from the values predicted on the basis of additivity towards lower values, the deviation increasing with increasing level of *rh* and filler loading [Figure 6(b)]. Suppression of polymer swelling,[19,36,46] responsible for the relatively high levels of hydration in neat PHEMA, and/or filler

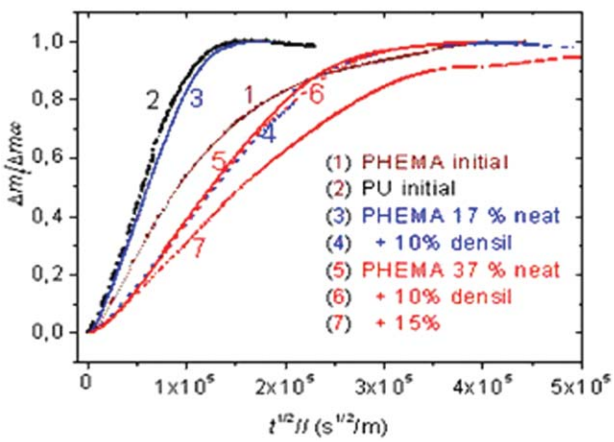

Figure 7. Dynamic desorption isotherms (DDI) for (1) neat PHEMA, (2) neat PU, (3) unfilled semi–IPN17, (4) semi–IPN17 + 10 wt % densil, (5) unfilled semi–IPN37, (6) semi–IPN37 + 10 wt % densil and (7) semi–IPN37 + 15 wt % densil. Water diffusion coefficient values, *D,* for desorption along with the values of time to equilibration of mass in ambience, t_{equil}, are listed on the plot. [Color figure can be viewed in the online issue, which is available at wileyonlinelibrary.com.]

aggregation, resulting in loss of primary hydration sites, could be at the origin of these results. Another striking result is that the experimental data for nanocomposites agree very well with those of calculations made by assuming no water sorption by silica (not shown), that is, by normalizing the experimental data to the semi–IPN content. A manifestation of that is the close proximity of water sorption data for 5 and 15% silica in Figure 6(b). It is interesting to note that similar observations were made in a previous work in nanocomposites based on crosslinked poly(hydroxyethyl acrylate) (PHEA) as matrix and silica *in situ* generated by sol–gel method as filler.[19] These results suggest that loss of hydration sites of silica because of both aggregation and hydrogen bonding interaction with PHEMA is the explanation for the lower experimental water uptakes of the nanocomposites at high levels of *rh* and loading as compared to additivity values in Figure 6(b). We will come back to this point in the next paragraph. Furthermore, we can follow in Figure 6(c,d) that the hydrophilicity of semi–IPNs with of PHEMA fractions tends to increase, in general, with addition of filler, showing maxima at 3 and 5 wt % of filler, for 17 and 37 wt % PHEMA, respectively, while at higher loadings hydrophilicity decreases. Thus, for the semi–IPNs these filler fractions seem critical. A possible explanation, supported also by SAXS and AFM results, is that at filler fractions lower than these filler contents densil nanoparticles are finely distributed within the polymer matrix, whereas at higher filler fractions aggregates are formed. Formation of aggregates has two diverse influences on water uptake. On the one hand, potential primary sorption sites, such as hydroxyls on silica surface, become no more accessible to water, so that water uptake decreases. On the other hand, the stiffening effect of the filler on the polymer matrix decreases, so that water uptake increases. The results in Figure 6(c,d) suggest that the first effect dominates over the second one in the nanocomposites based on semi–IPNs, whereas the opposite is true for the nanocomposites based on PU, more clearly at the intermediate *rh* values [i.e., ∼43 *rh*% in Figure 6(c)] where possible swelling effects of the polymer are not significant. Based on DSC results (Table II) suggesting that PHEMA interacts strongly with silica, we should modify the above conclusion by adding loss of hydration sites on silica by hydrogen bonding PHEMA-silica interactions next to that by silica aggregation. As a result, water uptake decreases with increasing silica content, in particular at high *rh* values, due to increased stiffening of the polymer matrix additionally.

It is interesting to compare the results presented here with those obtained with nanocomposites based on similar polymer matrices and silica in previous work. In the nanocomposites mentioned above based on crosslinked PHEA as matrix and silica *in situ* generated by sol–gel method as filler it was observed that the water uptake is practically the same as in pure PHEA at low silica contents, whereas it is reduced at higher silica contents, in particular at high *rh* values where swelling becomes significant.[19] Comparing with predicted values on the basis of additivity, it was observed that the measured water uptake was lower than the predicted one at all values of relative humidity, the difference being larger for higher silica contents. Thus, the results obtained with the PHEA/silica nanocomposites are similar to those obtained in the present work, in particular in semi–IPNs. Finally, in nanocomposites based on copolymers of PHEA and hydrophobic poly(ethyl acrylate) (PEA) the water uptake at fixed silica content was found to decrease with increasing PEA content, similar to the results obtained here with the two semi-IPNs.[46] Regarding the effect of silica at fixed copolymer composition, water uptake was practically independent of silica content at *rh* values lower than about 0.75, whereas it was reduced with increasing silica contents at higher *rh* values.

Diffusion of Water Molecules during Isothermal Desorption (DDI). Figure 7 shows representative results of dynamic desorption experiments for neat PHEMA, neat PU, semi–IPNs and the three types of nanocomposites with high amounts of densil. All values of water diffusion coefficient calculated by eq. (3) from these dynamic measurements along with hydration values on dry basis, $h_{dry,basis}$, calculated by eq. (2) for samples equilibrated at 95 *rh*% and in ambience (∼40 *rh*%) are given in Table III.

Within experimental error on D (∼10%), D value for the unfilled semi–IPN17 (17×10^{-8} cm^2/s) is quite similar to that of PU (20×10^{-8} cm^2/s), while D value for unfilled semi–IPN37 (5×10^{-8} cm^2/s) is lower by 60–75% and closer to neat PHEMA (7×10^{-8} cm^2/s).

At this point we should note that highly hydrated PHEMA is at rubber state (optical observation) while during dehydration (desorption) the polymer is deplasticized (T_g increases) changing to the glassy state. It is well known that diffusion of water molecules is significantly more difficult through a glassy material, as compared to the same materias in the rubbery state.[36]

As a result, diffusion coefficients, determined in a desorption experiment at high water contents, may depart from equilibration times, as indicated by the results in Table III. Thus, time to equilibration (maximum of desorption), t_{equil}, was found very high for neat PHEMA (∼100 hours, Table III, Figure 7). D is

Table III. Parameters from ESI and DDI Measurements at Room Temperature: Hydration on Dry Basis, $h_{dry,basis}$, for Samples Equilibrated at 95 *rh*% and in the Ambience (∼40 *rh*%), Water Diffusion Coefficient of Desorption, *D*

Sample	$H_{dry,basis}$ (95 rh %), wt	$h_{dry,basis}$ (amb.), wt	Diffusion coefficient, D, cm^2/s
PHEMA neat	0.18	0.03	7×10^{-8}
PU neat	0.04	0.01	20×10^{-8}
PU + 5% densil	0.04	0.01	5×10^{-8}
PU + 10% densil	0.04	0.01	4×10^{-8}
PU + 15% densil	0.04	0.01	3×10^{-8}
semi-IPN17 neat	0.06	0.02	$17 x10^{-8}$
semi-IPN17 + 5% densil	0.06	0.02	3×10^{-8}
semi-IPN17 + 10% densil	0.06	0.02	4×10^{-8}
semi-IPN17 + 15% densil	0.06	0.02	5×10^{-8}
semi-IPN37 neat	0.08	0.02	5×10^{-8}
semi-IPN37 + 5% densil	0.10	0.02	4×10^{-8}
semi-IPN37 + 10% densil	0.09	0.02	4×10^{-8}
semi-IPN37 + 15% densil	0.09	0.02	2×10^{-8}

* $H_{dry,basis}$ (95 rh %) measured with accuracy 0.01.
** $h_{dry,basis}$ (amb.) measured with accuracy 0.01.
*** D calculated with accuracy 1×10^{-8}.

lower and, respectively, t_{equil} is higher for semi–IPN37, as compared to PU and semi–IPN17. This is a strong indication of better mixing of PHEMA with PU in semi–IPN37, in agreement to AFM.

It is interesting to compare the water diffusion coefficient results reported above with similar results obtained with other PUs, IPNs and silica nanocomposites. The *D* values for the PU under investigation are similar to values obtained with linear PUs and in PUs based on poly(ethylene adipate), 4,4'–diphenylmethane diisocyanate and 1,4–butanediol, typical for water and for organic vapors in various linear polymers in the rubbery state.[66] Concerning the comparison between PU and the semi–IPN, lower *D* values were actually expected for the semi–IPN, because of the higher hydrophilicity of PHEMA.

Measurements in sequential poly(methyl acrylate)–poly(hydroxyethyl acrylate) (PMA–PHEA) IPNS showed higher *D* values in the hydrophobic PMA as compared to the hydrophilic PHEA (by one order of magnitude) and values in between, but closer to those of PHEA, in the microphase separated IPNs.[66]

Finally, we discuss the effect of filler on diffusion coefficient *D* (Table III). The results listed in Table III suggest that the presence of silica decreases strongly *D* of PU, due to higher hydrophilicity of densil. Systematic suppression of *D* with densil is also observed for semi–IPN37 based nanocomposites. Simultaneously, we observe a significant increase on t_{equil} as a result of PHEMA deplasticization, as described above. The same effect does not seem to rule the changes recorded for semi–IPN17, while t_{equil} values are lower and *D* does not change systematically with filler loading. Moreover, *D* of semi–IPN17 (17×10^{-8} cm^2/s) decreases to 3–5 $\times 10^{-8}$ cm^2/s in the nanocomposites. Bearing in mind that $h_{dry,basis}$ for 95 *rh*% and ambient *rh*% (Table III) are both lower than those of semi–IPN37 and almost unchanged with densil loading for semi–IPN17, the above result is most probably an effect of formation of surface layers of PHEMA on the nanoparticles of densil with high density and with hydrogen bonding with the surface.

CONCLUSIONS

Nanocomposites based on a sequential PU–PHEMA semi–IPN with 17 and 37 wt % of PHEMA filled with mechanochemically activated nanosilica were prepared and investigated in the perspective of biomedical applications. The investigation involved structure (SAXS), surface morphology (AFM), mechanical properties (stress–strain), calorimetry (DSC), molecular dynamics (DRS, TSDC) and hydration techniques. Special attention has been paid to the investigation of the hydration properties of the prepared materials, more specifically to the effects of sorbed water on the properties of the polymer matrix, by equilibrium and dynamic hydration/dehydration (ESI, DDI) techniques.

DSC and DRS results showed the existence of two polymer phases in the semi-IPNs. AFM and hydration results, in combination with specific observations by the other techniques, provided support for higher microphase separation in the semi-IPN with the higher PHEMA content (37 wt %). The respectively high T_g values for PHEMA and simultaneously the retarded diffusion of water molecules during desorption, both recorded higher for 37% PHEMA, could be the result of covalent bonding between hydroxyls of monomer HEMA and residual isocyanate groups of PU during the process of network formation resulting in grafting of HEMA on the polyurethane network.

According to SAXS and AFM, densil nanoparticles well distributed in the polymer matrix. It became possible due to asperity of surface of densil nanoparticles which allow adsorption of polymer chaines on the surface and as result – better distribution of nanoparticles in the polymer matrix. Nanoparticles were found partially aggregated for higher than 1, 3, and 5 wt % filler loading in PU, semi–IPN with 17 and 37 wt %, respectively.

The presence of nanoparticles were found suppressed polymer mobility (glass transition and molecular dynamics) of both PHEMA and PU, indicating interaction of densil with both polymers. The above effects were found significantly stronger for PHEMA phase. This is, in our opinion, the result of formation of surface layers of PHEMA on the nanoparticles of densil with high density and with hydrogen bonding with the surface.

The hydrophilicity properties of the semi-IPN is more or less preserved in the various nanocomposites or even enhanced in the case of non-aggregaded silica nanoparticles. The improvement of mechanical properties in combination with hydrophilicity and biocompatibility of nanocomposites are promising for use these materials for biomedical application namely as surgical films for wound treatment and as material for producing the medical devises.

ACKNOWLEDGMENTS

This research was partially supported by FP7—PIRSES–GA–2013–612484 NANOBIOMAT. This research has been co–financed by the European Union (European Social Fund—ESF) and Greek national funds through the Operational Program "Education and Lifelong Learning" of the National Strategic Reference Framework (NSRF)—Research Funding Program: Heracleitus II. Investing in knowledge society through the European Social Fund (P.K. and P.P.) and Research Funding Program: Aristeia (E.K, P.P., and E.S.).

AUTHOR CONTRIBUTIONS

Dr. Panagiotis Klonos supervised DSC, TSDC, DRS and hydration measurements and he contributed to the writing of the manuscript; Ms Vasileia Chatzidogiannaki performed the DSC and TSDC experiments; Mr Konstantinos Roumpos performed DRS and hydration measurements; Dr Ellas Spyratou performed the AFM measurements; Mr Panayiotis Georgiopoulos performed the stress–strain measurements, Prof Evagelia Kontou supervised and discussed the stress–strain properties; Prof Polycarpos Pissis supervised the research and contributed to the writing of the manuscript; Dr.Yuriy Gomza supervised and discussed SAXS results, Dr Stanislav Nesin performed SAXS experiments, PhD student Oksana Bondaruk performed samples preparation, Dr Lyudmyla Karabanova supervised the nanocomposite's synthesis and contributed to the writing of the manuscript.

REFERENCES

1. Paul, D. R.; Robenson, L. M. *J. Polym.* **2008**, *49*, 3187.
2. Jancar, J.; Douglas, J. F.; Starr, F. W.; Kumar, S. K.; Cassagnau, P.; Lesser, A. J.; Sternstein, S. S.; Buehler, M. J. *J. Polym.* **2010**, *51*, 3321.
3. Ray, S. S.; Okamoto, M. *J. Polym. Sci.* **2003**, *28*, 1539.
4. Alexandre, M.; Dubois, P. *J. Mater. Sci. Eng.* **2000**, *28*, 1.
5. Moniruzzaman, M.; Winey, K. I. *J. Macromol.* **2006**, *39*, 5194.
6. Shaffer, M. S. P.; Sandler, J. K. W. In Processing and Properties of Nanocomposites; Advani, S., Ed.; World Sci. Publ. Co. Pte. Ltd.: Singapore, **2006**; p. 31.
7. Bokobza, L.; Chauvin, J. P. *J. Polym.* **2005**, *46*, 4144.
8. Zou, H.; Wu, S.; Shen, J. *J. Chem. Rev.* **2008**, *108*, 3893.
9. Vo, L. T.; Anastasiadis, S. H.; Giannelis, E. P. *J. Macromol.* **2011**, *24*, 6162.
10. Takakashi, S.; Paul, D. R. *J. Polym.* **2006**, *47*, 7519.
11. Nodera, A.; Kanai, T. *J. Appl. Polym. Sci.* **2006**, *101*, 3862.
12. Papageorgiou, G. Z.; Terzopoulou, Z.; Bikiaris, D.; Triantafyllidis, K. S.; Diamanti, E.; Gournis, D.; Klonos, P.; Giannoulidis, E.; Pissis, P. *Thermochim. Acta* **2014**, *597*, 48.
13. Karabanova, L. V.; Whitby, R. L.; Korobeinyk, A.; Bondaruk, O.; Salvage, J.; Lloyd, A. W.; Mikhalovsky, S. V. *Compos. Sci. Technol.* **2012**, *72*, 865.
14. Gun'ko, V. M.; Voronin, E. F.; Nosach, L. V.; Pakhlov, E. M.; Guzenko, N. V.; Leboda, R.; Skubiszewska–Zięba, J. *Adsorpt. Sci. Technol.* **2006**, *24*, 143.
15. Mark, J. E.; Lee, C. Y. C. Hybrid Organic–inorganic composites; ACS Symp: Washington, **1995**.
16. Sysel, P.; Pulec, R.; Maryska, M. *Polym. J.* **1997**, *29*, 607.
17. Matejka, L.; Dusek, K.; Plestil, J.; Kriz, J.; Lednicky, L. *Polymer* **1998**, *40*, 171.
18. Bokobza, L.; Diop, A. L. *Express Polym. Lett.* **2010**, *4*, 355.
19. Pandis, C.; Spanoudaki, A.; Kyritsis, A.; Pissis, P.; Rodriquez Hernández, J. C.; Gómez Ribelles, J. L.; Monleón Pradas, M. *J. Polym. Sci., Part B: Polym. Phys.* **2011**, *49*, 657.
20. Klonos, P.; Panagopoulou, A.; Bokobza, L.; Kyritsis, A.; Peoglos, V.; Pissis, P. *Polymer* **2010**, *51*, 5490.
21. Stoeber, W.; Fink, A.; Bohn, E. *J. Colloid Interface Sci.* **1968**, *26*, 62.
22. Bershtein, V.; Gun'ko, V.; Egorova, L.; Guzenko, N.; Pakhlov, E.; Ryzhov, V.; Zarko, V. *Polymer* **2009**, *50*, 860.
23. Karabanova, L. V.; Boiteux, G.; Gain, O.; Seytre, G.; Sergeeva, L. M.; Lutsyk, E. D. *Polym. Intern.* **2004**, *53*, 2051.
24. Bolbukh, Y.; Tertykh, V.; Klonos, P.; Pissis, P. *J. Therm. Anal. Calorim.* **2012**, *108*, 1111.
25. Klonos, P.; Sulym, I. Y.; Borysenko, M. V.; Gun'ko, V. M.; Kripotou, S.; Kyritsis, A.; Pissis, P. *Polymer* **2015**, *58*, 9.
26. Galaburda, M. V.; Klonos, P.; Gun'ko, V. M.; Bogatyrov, V. M.; Borysenko, M. V.; Pissis, P. *Appl. Surf. Sci.* **2014**, *305*, 67.
27. Sulym, I.; Klonos, P.; Borysenko, M.; Pissis, P.; Gun'ko, V. M. *J. Appl. Polym. Sci.* **2014**, *131*, 41154.
28. Bershtein, V. A.; Gun'ko, V. M.; Karabanova, L. V.; Sukhanova, T. E.; Yakushev, P. N.; Egorova, L. M.; Glievyy, O. B.; Lutsyk, E. D.; Pakhlov, E. M.; Turova, A. A.; Zarko, V. I.; Vylegzhanina, M. E. *J. Macromol. Sci. Phys.* **2010**, *49*, 18.
29. Karabanova, L. V.; Bershtein, V. A.; Sukhanova, T. E.; Yakushev, P. N.; Egorova, L. M.; Lutsyk, E. D.; Svyatyna, A. V.; Vylegzhanina, M. E. *J. Polym. Sci., Part B: Polym. Phys.* **2008**, *46*, 1696.
30. Karabanova, L. V.; Boiteux, G.; Seytre, G.; Stevenson, I.; Lloyd, A. W.; Mikhalovsky, S. V.; Helias, M.; Sergeeva, L.

M.; Lutsyk, E. D.; Svyatyna, A. V. *Polym. Eng. Sci.* **2008**, *48*, 588.

31. Karabanova, L.; Pissis, P.; Kanapitsas, A.; Lutsyk, E. *J. Appl. Polym. Sci.* **1998**, *68*, 161.
32. Kanapitsas, A.; Pissis, P.; Karabanova, L.; Sergeeva, L.; Apekis, L. *Polym. Gels Network* **1998**, *6*, 83.
33. Karabanova, L. V.; Boiteux, G.; Seytre, G.; Stevenson, I.; Gain, O.; Shady, C.; Lutsyk, E. D.; Svyatyna, A. *J Non–Cryst. Solids* **2009**, *355*, 1453.
34. Stamatopoulou, C.; Klonos, P.; Koutsoumpis, S.; Gun'ko, V. M.; Pissis, P.; Karabanova, L. *J. Appl. Polym. Sci., Part B: Polym. Phys.* **2014**, *52*, 397.
35. Gun'ko, V. M.; Voronin, E. F.; Nosach, L. V.; Turov, V. V.; Wang, Z.; Vasilenko, A. P.; Leboda, R.; Skubiszewska–Zięba, J.; Janusz, W.; Mikhalovsky, S. V. *J. Colloid Interface Sci.* **2011**, *355*, 300.
36. Pissis, P.; Kyritsis, A. J. *Appl. Polym. Sci., Part B: Polym. Phys.* **2013**, *51*, 159.
37. Lipatov, Yu. S.; Shilov, V. V.; Gomza, Yu. P.; Kruglyak, N. E. X-Ray Diffraction Methods for the Study of Polymer Systems; Naukova Dumka: Kiev, **1982**; p 296.
38. Vonk, C. G. *J. Appl. Cryst.* **1974**, *8*, 340.
39. Hosemann, R.; Bagchi, S. N. Direct Analysis of Diffraction by Matter; North Holland Co: Amsterdam, **1962**; p 656.
40. Wiesendanger, R. Scanning Probe Microscopy and Spectroscopy: Methods and Applications; Cambridge University Press: Cambridge, **1994**; p 637.
41. Sakurai, T.; Watanabe, Y. Advances in Scanning Probe Microscopy in Advances in Materials Research; Springer Verlag: London, **2000**.
42. Kontou, E.; Farasoglou, P. *J. Mater. Sci.* **1998**, *33*, 147.
43. Georgiopoulos, P.; Kontou, E.; Niaounakis, M. *Polym. Compos.* **2014**, *35*, 1140.
44. Vanderschueren, J.; Gasiot, J. Thermally Stimulated Relaxation in Solids; Brauenlich, P., Ed.; Springer: Berlin, **1979**; Vol. *37*, Chapter 4, pp 135–223.
45. Kremer, F.; Schönhals, A. Broadband Dielectric Spectroscopy; Springer Verlag: Berlin, **2003**.
46. Stathopoulos, A.; Klonos, P.; Kyritsis, A.; Pissis, P.; Christodoulides, C.; Rodriquez Hernández, J. C.; Monleón Pradas, M.; Gómez Ribelles, J. L. *Eur. Polym. J.* **2010**, *46*, 101.
47. Greenspan, L. *J. Res. Natl. Bur., Stand A: Phys. Chem.* **1977**, *81*, 89.
48. Crank, J.; Park, G. S. Diffusion in Polymers; Academic Press: London, **1968**; p 1.
49. Shilov, V. V.; Karabanova, L. V.; David, L.; Boiteux, G.; Seytre, G.; Gomza, Y. P.; Nesin, S.; Sergeeva, L. M.; Lutsyk, E. D.; Svyatyna, A. B. *Polymerny Zurnal* **2005**, *27*, 255.
50. Beaucage, G. *J. Appl. Cryst.* **1995**, *28*, 717.
51. Beaucage, G. *J. Appl. Cryst.* **1996**, *29*, 134.
52. Gin'e, A. X-ray-Analysis of Crystals. Theory and Practice; Physicomathematical Publishers: Moscow, **1961**; p 604.
53. Gao, S. L.; Mader, E. *Composites* **2002**, *33*, 559.
54. Gao, S. L.; Mader, E.; Zhandarov, S. F. *Carbon* **2004**, *42*, 515.
55. Spyratou, E.; Asproudis, I.; Tsoutsi, D.; Bacharis, C.; Moutsouris, K.; Makropoulou, M.; Serafetinides, A. A. *Appl. Surf. Sci.* **2010**, *256*, 2539.
56. Rodriquez Hernández, J. C.; Monleón Pradas, M.; Gómez Ribelles, J. L. *J. Non–Cryst Solids* **2008**, *354*, 1900.
57. Raftopoulos, K. N.; Jancia, M.; Aravopoulou, D.; Hebda, E.; Pielichowski, K.; Pissis, P. *Macromolecules* **2013**, *46*, 7378.
58. Klonos, P.; Panagopoulou, A.; Kyritsis, A.; Bokobza, L.; Pissis, P. *J. Non–Cryst Solids* **2011**, *357*, 610.
59. Bershtein, V. A.; Gun'ko, V. M.; Karabanova, L. V.; Sukhanova, T. E.; Yakushev, P. N.; Egorova, L. M.; Turova, A. A.; Zarko, V. I.; Pakhlov, E. M.; Vylegzhanina, M. E.; Mikhalovsky, S. V. Royal Society Chemistry Advances: Britain, **2013**; Vol. 3, Chapter 34, pp 14560–14570.
60. Georgoussis, G.; Kanapitsas, A.; Pissis, P.; Savelyev, Y. V.; Veselov, V. Y.; Privalko, E. G. *Eur. Polym. J.* **2000**, *36*, 1113.
61. Havriliak, S.; Negami, S. *Polymer* **1967**, *8*, 161.
62. Fragiadakis, D.; Bokobza, L.; Pissis, P. *Polymer* **2011**, *52*, 3175.
63. Donth, E. The Glass Transition: Relaxation Dynamics in Liquids and Disordered Materials; Springer Series in Materials Science: Berlin, **2001**; p 419.
64. Bras, A. R.; Viciosa, M. T.; Wang, Y.; Dionisio, M.; Mano, J. F. *Macromolecules* **2006**, *39*, 6513.
65. Pissis, P.; Apekis, L.; Christodoulides, C.; Niaounakis, M.; Kyritsis, A.; Nedbal, J. *J. Polym. Sci., Part B: Polym. Phys.* **1996**, *34*, 1529.
66. Gomez Ribelles, J. L.; Monleon Pradas, M.; Gallego Ferrer, G.; Peidro Torres, N.; Perez Gimenez, V.; Pissis, P.; Kyritsis, A. *J. Polym. Sci., Part B: Polym. Phys.* **1999**, *37*, 1587.